Alexandria Engineering Journal (2016) 55, 2473–2483

HOSTED BY

ELSEVIER

Alexandria University

Alexandria Engineering Journal

www.elsevier.com/locate/aej
www.sciencedirect.com

REVIEW

Thermohydrodynamic analysis of airfoil bearing based on bump foil structure

S.Y. Maraiy *, W.A. Crosby, H.A. EL-Gamal

Department of Mechanical Engineering, Faculty of Engineering, Alexandria University, Alexandria, Egypt

Received 27 April 2016; revised 23 May 2016; accepted 4 June 2016
Available online 10 August 2016

KEYWORDS

Foil bearings;
Thermohydrodynamic analysis;
Bump foil structure

Abstract The load carrying capacity of the gas foil bearing depends on the material properties and the configuration of the underlying bump strip's structure. This paper presents three different cases for selecting the dimensions of the foil bearing to guarantee the highest possible load carrying capacity. It focuses on three main parameters that affect the compliance number; these parameters are the length of bump in θ direction, the pitch of bump foil, and the thickness of bump foil. It also studies the effect of changing these parameters on load carrying capacity according to both isothermal and thermohydrodynamic approaches.

Contents

* Corresponding author.
E-mail address: sabrien_maraiy@yahoo.com (S.Y. Maraiy).

Peer review under responsibility of Faculty of Engineering, Alexandria University.

http://dx.doi.org/10.1016/j.aej.2016.06.015

Nomenclature

a	viscosity constant of air, Pa s/°C
b	bearing width, m
C	radial clearance, m
C_p	specific heat at constant pressure, J/kg K
d	distance between bumps, m
D	bearing diameter, m
D_h	housing diameter, m
e	eccentricity, m
E	modulus of elasticity, Pa
h	fluid film thickness, m
$\bar{h}$	dimensionless air film thickness, $\frac{h}{C}$
h_b	bump height, m
$h_{\min}$	minimum film thickness, m
$\bar{h}_{\mathrm{cr}}$	dimensionless film thickness at $\theta = \theta_{\mathrm{cr}}$
J	number of iterations of the matlab program
K	constant reflecting the structure rigidity of the bumps, m^3/N
K_a	conductivity of air, W/K m
l	half length of bump in θ direction, m
L	bearing length, m
n	number of bumps
p	fluid film pressure, Pa
$\bar{P}$	dimensionless hydrodynamic pressure, $\bar{P} = \frac{p}{p_a}$
p_a	ambient pressure, Pa
Q_{rec}	recirculating flow rate, kg/s
Q_{suc}	suction flow rate, kg/s
r	radius of bump, m
r_o	radius of spindle, m
R	radius of shaft, m
S	pitch of bump foil, m
t_b	thickness of bump foil, m
T	temperature of gas, °C
T_a	ambient temperature of the air, °C
T_{in}	inlet temperature of the gas film, °C
T_{ref}	reference temperature, °C
u	linear velocity of shaft speed, m/s
v	linear velocity of gas flow in axial, y, direction, m/s
w	linear velocity of gas flow in z direction, m/s
W	bearing load carrying capacity, W_x, W_z, components, N
W_t	radial deformation of the bump foil due to the steady-state aerodynamic pressure, m
$\bar{W}_x$	non dimensionless load component in the direction of foil movement, $\bar{W}_x = \frac{W_x}{P_a RL}$
$\bar{W}_z$	non dimensionless load component in axial length direction, $\bar{W}_z = \frac{W_z}{P_a RL}$
x	Cartesian coordinate in the direction of motion
y	Cartesian coordinate across the film thickness
z	coordinate in axial length direction, m
$\bar{z}$	dimensionless coordinate in axial length direction, $\bar{Z} = \frac{Z}{L/2}$

Greek symbols

α	bump foil compliance number
α_v	coefficient of cubic expansion
β	wrap angle, °
δ	bearing liner deformation, m
ε	eccentricity ratio, $\varepsilon = \frac{e}{C}$
θ	angular coordinate in the direction of motion
θ_{cr}	critical value of θ at subambient hydrodynamic pressure
Λ	bearing number, $\Lambda = \frac{6\mu_a \omega}{P_a}\left(\frac{R}{C}\right)^2$
μ	absolute viscosity of the fluid, N s/m^2
μ_a	viscosity of air, N s/m^2
υ	Poisson ratio
ρ	density, kg/m^3
φ	attitude angle, °
ψ	bump arc angle, °
ω	angular velocity of the shaft, rad/s

Subscripts

a	ambient, bearing entrance conditions
x, y, z	quantities in the x, y, or z directions
r, θ	quantities in the r or θ directions
v	volume
t	time

Overbar

$\overline{(\mathrm{symbol})}$	non-dimensionalized parameters

1. Introduction

In recent years, foil bearings have gained more attention than any other types of bearings because of their unique mode of operation and diversity of applications. They also have various advantages compared to the conventional rigid journal bearings in terms of higher load carrying capacity, lower power loss, better stability, and greater endurance. These bearings are self-acting, and can operate with ambient air or any processing gas as the lubricating fluid.

Their assembly includes a first thin smooth compliant sheet facing the shaft, one or more corrugated foil, a second sheet between the foils and a compliant sheet for preventing sagging of the first sheet between ridges of foil. Under the action of the hydrodynamic pressure, the foil structure deforms. Therefore, the fluid film pressure must be coupled to the deformation of the foil structure in order to know the characteristics of the foil bearing performance. From this point of view, many analytical studies have been conducted based on a range of structural models.

The concept of a foil bearing was first described in a report over 50 years ago by Blok and Van Rossum [1]. In 1957, Patel and Cameron [2] followed this work with another experimental investigation using steel tape and oil by introducing a more elaborate differential equation for finite width and derived a less restrictive differential equation for the gap thickness than Blok and Van Rossum [1].

In 1962, Gross [3] introduced the differential equations for a tape transport with air as a lubricant. In 1965, Eshel and Elrod [4] rederived the differential equation of Blok and Van Rossum [1] and presented a more refined and elaborate solution for the nominal gap width than those already mentioned. They also presented numerical solutions for the film thickness of the infinitely wide, self-acting foil bearing for various values of tape stiffness [5].

Eshel [6] studied the effect of compressibility on foil bearings and he found that, with increasing compressibility, the nominal clearance decreased and the exit undulation decreased in amplitude and increased in wavelength until it completely disappeared. In 1970, he [7] also, showed that the air film, due to self-acting lubrication effects, could be sharply reduced by small corners in the solid over which the foil passes. He investigated some factors useful in overcoming excessive air gaps in foil bearings.

Heshmat et al. [8] studied the gas-lubricated foil journal bearings, and evaluated its performance using a spring supported compliant foil as the bearing surface.

In 1986, Crosby [9] made a study to understand and quantify the performance of an oil-lubricated ridged foil journal bearing of finite length and lubricated with an incompressible fluid. He found that by decreasing the stiffness of bearing, the film pressure decreased and, consequently, the bearing load for the ridged bearing was shown to be less than that for the rigid bearing for the same eccentricity.

Ku and Heshmat [10] developed a method to obtain the stiffness of a compliant foil bearing and found that it depended on several parameters such as the bump configuration, surface coating and the presence or absence of lubrication. In the same sense, Ku [11] described the effects of bearing parameters, such as static loads, dynamics displacement amplitudes, bumps configurations, pivot locations and surface coating in the dynamic characteristics of foil bearings. In 1994, Ku and Heshmat [13] presented a theoretical model to predict the structural stiffness and damping coefficients of the bump foil strip in a journal bearing or damper. They found, theoretically, that the energy dissipated from this loop was mostly contributed by the frictional motion between contact surfaces. In [14] they presented the results of the second part of the investigation on structural stiffness and coulomb damping in compliant foil journal bearings.

Peng and Khonsari [17] developed a model to predict the hydrodynamic performance of a foil journal bearing accounting for both the compressibility of air and the compliance of the bearing surface. They presented a series of predictions of the load-carrying capacity based on the numerical solution for pressure using a wide range of operating speeds. The results showed good agreement with existing experimental data. They [18] developed a thermohydrodynamic model for predicting the three-dimensional (3D) temperature field in an air-lubricated, compliant foil journal bearing. The model accounted for the compressibility and the viscosity-temperature characteristic of air and the compliance of the bearing surface.

Kuznetsov [19] has developed a numerical THD model to investigate the effect of lining compliance on the bearing characteristics. The analysis showed increased load carrying capacity, significantly reduced peak pressures and thicker oil film in the loaded zone compared to a white metal bearing. Slightly thinner oil films were predicted at the bearing edges. It was also shown that load carrying capacity was more sensitive to thermal expansion while pressure and oil film thickness profiles were more sensitive to elastic deformation.

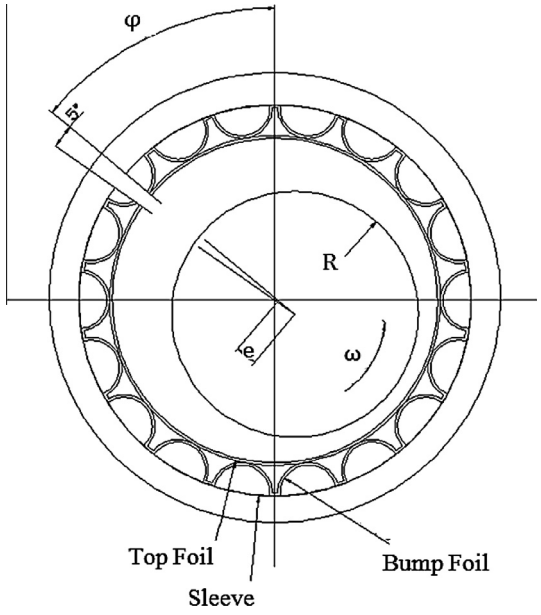

Figure 1 Schematic of compliant journal bearing.

2. Modeling of foil support structure

The structure of bump foil bearing is shown in Fig. 1. It is comprised of a bearing sleeve lined with corrugated bumps (bump foil), the leading edges of both bump and top foil are

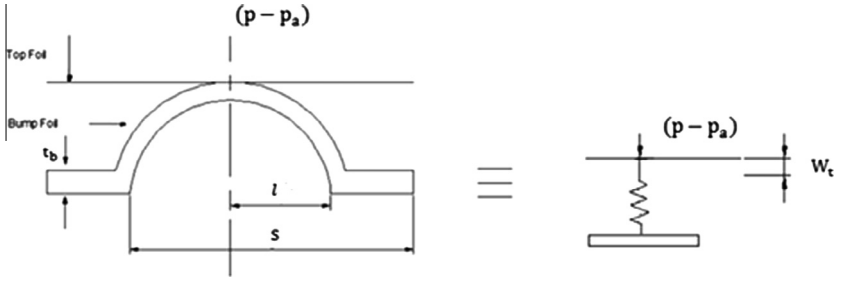

Figure 2 Single segment of bump foil.

spot-welded to the bearing sleeve, the trailing edges of foils are free, and bump foils support the single flat top foil.

The bump foils acting as springs provide stiffness, and the smooth top foil layer provides the bearing surface. When the shaft rotates over one certain speed, the top foil expands outward, and the air film is generated, and the shaft is then separated from the top foil.

The elastic support structure considered in the present analysis is a simple foundation model, according to the original work of Heshmat et al. [8] which most of the published models are based on. This analysis relies on several assumptions which other researchers have also reproduced:

(1) The stiffness of a bump strip is uniformly distributed throughout the bearing surface, i.e. the bump strip is regarded as a uniform elastic foundation.
(2) Bump stiffness is constant, independent of the actual bump deflection, not related to or constrained by adjacent bumps.
(3) The top foil does not sag between adjacent bumps. The top foil does not have either bending or membrane stiffness, and its deflection follows that of the bump.

With these considerations, the radial deformation of the bump foil due to the steady-state aerodynamic pressure (W_t) depends on the bump compliance (α) and the average pressure across the bearing width as shown in Fig. 2:

$$W_t = K(p - p_{a)} \tag{1}$$

where p and p_a are the steady-state gas-film pressure and the ambient pressure, respectively and K is a constant reflecting the structure rigidity of the bumps. It was shown in [6] that K is given by

$$K = \frac{\alpha C}{p_a} \tag{2}$$

where

$$\alpha = \frac{2p_a S}{CE}\left(\frac{l}{t_b}\right)^3 (1 - \upsilon^2) \tag{3}$$

In order to study the performance of the foil bearing, we should first be able to select its dimensions. Eq. (3) shows that there are two main parameters that affect the compliance number, l the half length of bump in θ direction and S the pitch of bump foil, so we should carefully select them.

3. Thermohydrodynamic analysis

In a THD analysis, we deal with a compressible fluid; also the energy equation and the Reynolds' equation are coupled through the lubricant's viscosity-temperature relationship. These interdependences require simultaneous treatment of both equations to arrive at a final solution for pressure and temperature.

3.1. Numerical analysis of generalized Reynolds' equation

In order to study the variation of the air viscosity with temperature a generalized form of Reynolds' equation is developed where the variation of μ not only in the x and z directions but also in the y direction is considered.

The generalized Reynolds' equation is as follows:

$$\frac{\partial}{\partial x}\left[F_2\frac{ph^3}{\mu}\frac{\partial p}{\partial x}\right] + \frac{\partial}{\partial z}\left[F_2\frac{ph^3}{\mu}\frac{\partial p}{\partial z}\right] = \frac{\partial}{\partial x}\left[\left(F_4 - \frac{F_3}{F_o}\right)u\right] + \frac{\partial}{\partial z}\left[\left(F_4 - \frac{F_3}{F_o}\right)w\right] \tag{4}$$

where

$$F_o = \int_0^h \frac{dy}{\mu}, \quad F_1 = \int_0^h \frac{ydy}{\mu},$$

$$F_2 = \frac{F_1}{F_o}F_3 - \int_0^h \rho \int_0^y \frac{ydy}{\mu}dy$$

$$F_3 = \int_0^h \rho \int_0^y \frac{ydy}{\mu}dy, F_4 = \int_0^h \rho dy$$

If the variation in the lubricant's density is neglected, the generalized Reynolds equation in dimensionless form could be written in the following normalized form [20]:

$$\frac{\partial}{\partial\theta}\left[I_2\bar{P}\bar{h}^3\frac{\partial\bar{P}}{\partial\theta}\right] + \left(\frac{D}{L}\right)^2\frac{\partial}{\partial\bar{Z}}\left[I_2\bar{P}\bar{h}^3\frac{\partial\bar{P}}{\partial\bar{Z}}\right] = \Lambda\bar{\mu}\frac{\partial}{\partial\theta}\left(\bar{P}\bar{h}\left(1 - \frac{I_1}{I_o}\right)\right) \tag{5}$$

where

$$I_o = \int_0^1 \frac{d\bar{y}}{\bar{\mu}}, \quad I_1 = \int_0^1 \frac{\bar{y}d\bar{y}}{\bar{\mu}}, \quad I_2 = \int_0^1 \frac{\bar{y}}{\bar{\mu}}\left(\bar{y} - \frac{I_1}{I_o}\right)d\bar{y}$$

$$\bar{h} = 1 + \varepsilon\cos\theta + \alpha(\bar{P} - 1)$$

The appropriate boundary conditions for the Reynolds' equation are as follows:

$$\bar{P} = 1 \text{ at } \bar{Z} = \pm 1$$

$$\frac{\partial\bar{P}}{\partial\bar{Z}} = 0 \text{ at } \bar{Z} = 0$$

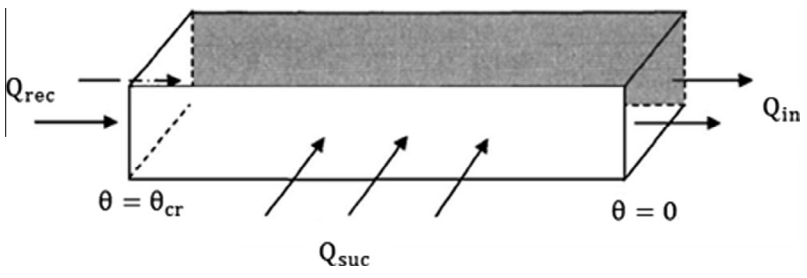

Figure 3 Schematic of the region where recirculating air mixes with fresh air [18].

$$\bar{P}(\theta = 0) = \bar{P}(\theta = \theta_{\text{end}})$$

where θ_{end} is the circumferential angle at which the top foil ends as shown in Fig. 2.

Typically, $\theta_{\text{end}} = 355^{\circ}$ [60].

The third boundary condition states that the pressure is periodic in the circumferential direction.

Using the finite difference method to solve Eq. (5) and simplifying, the equation will be as follows:

$$\bar{h}_{i,j}^3 I_2 \left[\frac{2}{(\Delta\theta)^2} + \left(\frac{D}{L}\right)^2 \frac{2}{(\Delta\bar{z})^2}\right]\overline{P}_{i,j}^2 + \left[\frac{-\bar{h}_{i,j}^3 I_2 \overline{P}_{i+1,j} - \bar{h}_{i,j}^3 I_2 \overline{P}_{i-1,j}}{(\Delta\theta)^2} - \left(\frac{D}{L}\right)^2 \frac{\bar{h}_{i,j}^3 I_2 \overline{P}_{i,j+1} + \bar{h}_{i,j}^3 I_2 \overline{P}_{i,j-1}}{(\Delta\bar{z})^2} + \Lambda\bar{\mu}\left(1 - \frac{I_1}{I_o}\right)\frac{\bar{h}_{i+1,j} - \bar{h}_{i-1,j}}{2\Delta\theta}\right]\overline{P}_{i,j}$$
$$+ \left[\bar{h}_{i,j}^3 I_2 \frac{\left(\overline{P}_{i+1,j} - \overline{P}_{i-1,j}\right)^2}{4(\Delta\theta)^2} - \left(\frac{D}{L}\right)^2 \bar{h}_{i,j}^3 I_2 \frac{\left(\overline{P}_{i,j+1} - \overline{P}_{i,j-1}\right)^2}{4(\Delta\bar{z})^2} + \Lambda\bar{\mu}\left(1 - \frac{I_1}{I_o}\right)\bar{h}_{i,j}\frac{\overline{P}_{i+1,j} - \overline{P}_{i-1,j}}{2\Delta\theta}\right] = 0 \tag{6}$$

3.2. Energy equation

The temperature distribution is determined from the energy equation. For an incompressible flow the equation is

$$\rho c_p\left(u\frac{\partial T}{\partial x} + v\frac{\partial T}{\partial y} + w\frac{\partial T}{\partial z}\right) = K_a\frac{\partial^2 T}{\partial x^2} + K_a\frac{\partial^2 T}{\partial y^2} + K_a\frac{\partial^2 T}{\partial z^2} + u\frac{\partial P}{\partial x} + v\frac{\partial P}{\partial y} + w\frac{\partial P}{\partial z} + \mu\left[\left(\frac{\partial u}{\partial y}\right)^2 + \left(\frac{\partial w}{\partial y}\right)^2\right] \tag{7}$$

The viscosity-temperature relationship of air is given by Salehi et al. [22]:

$$\mu = a(T - T_{\text{ref}})$$

where a is viscosity constant of air $= 4 \times 10^{-4}$ Pa s/°C and $T_{ref} = -458.75$ °C when T is in °C.

To solve Eq. (7) we assume heat convection along θ and y directions only and assume heat conduction along y direction only.

By using dimensionless parameters, Eq. (7) will be as follows:

$$K_1\left(\bar{u}\frac{\partial\overline{T}}{\partial\theta} + \frac{\bar{v}}{\bar{h}}\frac{\partial\overline{T}}{\partial\bar{y}}\right) = K_2\frac{1}{\bar{h}^2}\frac{\partial^2\overline{T}}{\partial\bar{y}^2} + K_3\left(\bar{u}\frac{\partial\bar{P}}{\partial\theta} + \bar{v}\frac{1}{\bar{h}}\frac{\partial\bar{P}}{\partial\bar{y}} + \bar{w}\left(\frac{D}{L}\right)\frac{\partial\bar{P}}{\partial\bar{z}}\right) + K_4\bar{\mu}\frac{1}{\bar{h}^2}\left[\left(\frac{\partial\bar{u}}{\partial\bar{y}}\right)^2 + \left(\frac{\partial\bar{w}}{\partial\bar{y}}\right)^2\right] \tag{8}$$

where $K_1 = \frac{\rho c_p U T_a}{R}$, $K_2 = \frac{K_a T_a}{C^2}$, $K_3 = \frac{U P_a}{R}$, $K_4 = \frac{\mu_a U^2}{C^2}$.

The velocity fields in dimensionless form are given by [21]

$$\bar{u} = 6\frac{\bar{h}^2}{\Lambda}\frac{\partial\bar{p}}{\partial\theta}\left[\int_0^{\bar{y}}\frac{\bar{y}}{\bar{\mu}}d\bar{y} - \frac{I_1}{I_o}\int_0^{\bar{y}}\frac{1}{\bar{\mu}}d\bar{y}\right] - 1 + \frac{1}{I_o}\int_0^{\bar{y}}\frac{1}{\bar{\mu}}d\bar{y} \tag{9}$$

$$\bar{v} = -\bar{u}\bar{\mu}\frac{\partial\bar{h}}{\partial\theta} \tag{10}$$

$$\bar{w} = 6\left(\frac{D}{L}\right)\frac{\bar{h}^2}{\Lambda}\frac{\partial\bar{p}}{\partial\bar{z}}\left[\int_0^{\bar{y}}\frac{\bar{y}}{\bar{\mu}}d\bar{y} - \frac{I_1}{I_o}\int_0^{\bar{y}}\frac{1}{\bar{\mu}}d\bar{y}\right] + \frac{1}{I_o}\int_0^{\bar{y}}\frac{1}{\bar{\mu}}d\bar{y} \tag{11}$$

The finite difference method form of Eq. (8) is

$$\left(\frac{K_1\bar{u}}{\Delta\theta} + \frac{K_1\bar{v}}{\bar{h}_{i,j}\Delta y} - \frac{K_2}{\bar{h}^2(\Delta y)^2}\right)\bar{T}_{i,k} = K_2\frac{1}{\bar{h}^2}\frac{\bar{T}_{i,k-2} - 2\bar{T}_{i,k-1}}{(\Delta y)^2} + \frac{K_1\bar{u}}{\Delta\theta}\bar{T}_{i-1,k} + \frac{K_1\bar{v}}{\bar{h}_{i,j}\Delta y}\bar{T}_{i,k-1} + K_3\left(\bar{u}\frac{\overline{P}_{i+1,j} - \overline{P}_{i-1,j}}{2\Delta\theta} + \bar{v}\frac{1}{\bar{h}}\frac{\partial\overline{P}}{\partial\bar{y}} + \bar{w}\left(\frac{D}{L}\right)\frac{\overline{P}_{i,j+1} - \overline{P}_{i,j-1}}{2\Delta z}\right) + K_4\bar{\mu}_{i,k}\frac{1}{\bar{h}^2}\left[\left(\frac{\partial\bar{u}}{\partial\bar{y}}\right)^2 + \left(\frac{\partial\bar{w}}{\partial\bar{y}}\right)^2\right] \tag{12}$$

Eq. (12) is to be solved using the following boundary condition:

$T = T_{\text{in}}$, where T_{in} is the inlet temperature of air °C

Table 1 Bearing data.

Bearing radius, $R = D/2$	$35 * 10^{-3}$ m
Bearing length, L	$70 * 10^{-3}$ m
Bearing clearance, C	$35 * 10^{-6}$ m
Bump foil Young's modulus, E_b	$207 * 10^9$ N/m^2
Bump foil Poisson's ratio, υ	0.3

Table 2 Lubricant (air) data.

Viscosity of air, μ_a	$1.932 * 10^{-5}$ Pa s
Lubricant density, ρ	1.1614 kg/m^3
Specific heat of air, C_p	1007 J/kg K
Air conductivity, K_a	$2.63 * 10^{-2}$ W/m K
Shaft angular speed, ω	30,000 rpm

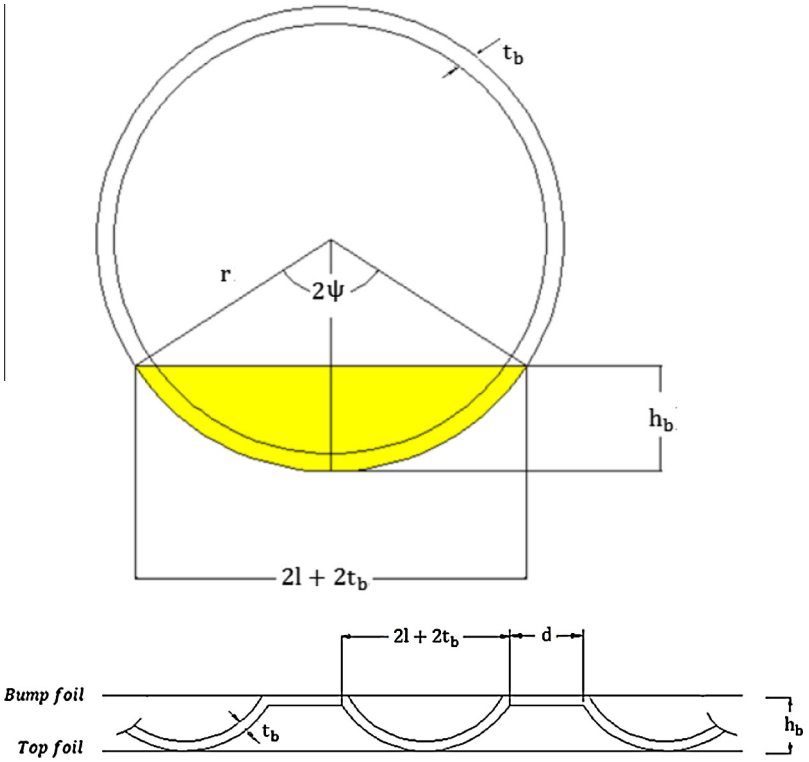

Figure 4 Configuration of bumps.

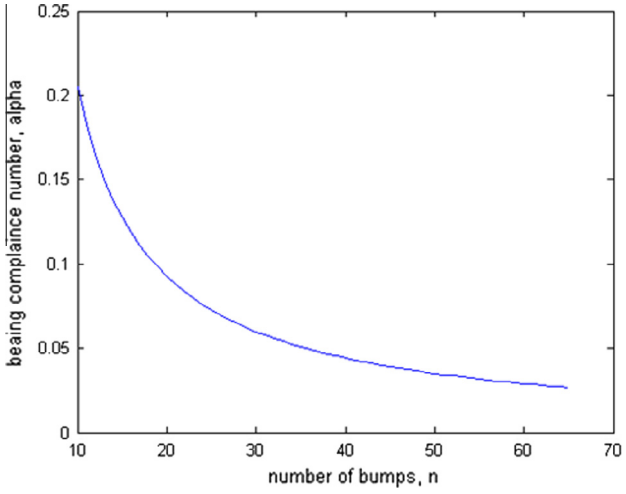

Figure 5 Effect of increasing number of bumps on compliance number (Case One).

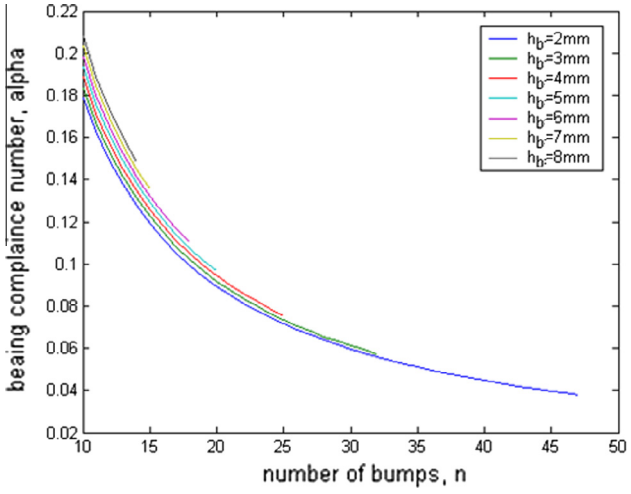

Figure 6 Effect of changing bump height on bearing compliance number.

The parameter T_{in} represents the temperature at $\theta = 0$, i.e., the "inlet" temperature. Since the recirculating air temperature is generally greater than that of the fresh air entering the bearing, a mixing temperature must be calculated for T_{in}. The mixing temperature represents the effective temperature after the warm air mixes with the fresh air. A simple schematic of the control volume representing the region where the air mixes is shown in Fig. 3.

An energy balance in this control volume is given by

$$\bar{T}_{in} = \frac{\bar{T}_{rec}\bar{Q}_{rec} + \bar{T}_{suc}\bar{Q}_{suc}}{\bar{Q}_{rec} + \bar{Q}_{suc}} \tag{13}$$

where

$$\bar{Q} = Q/Q_{ref} \text{ and } Q_{ref} = \frac{P_a C^3}{\mu_a}\left(\frac{D}{L}\right)$$

where $\bar{Q}_{rec}$ is the recirculating flow calculated using the following integration (Eq. (14)):

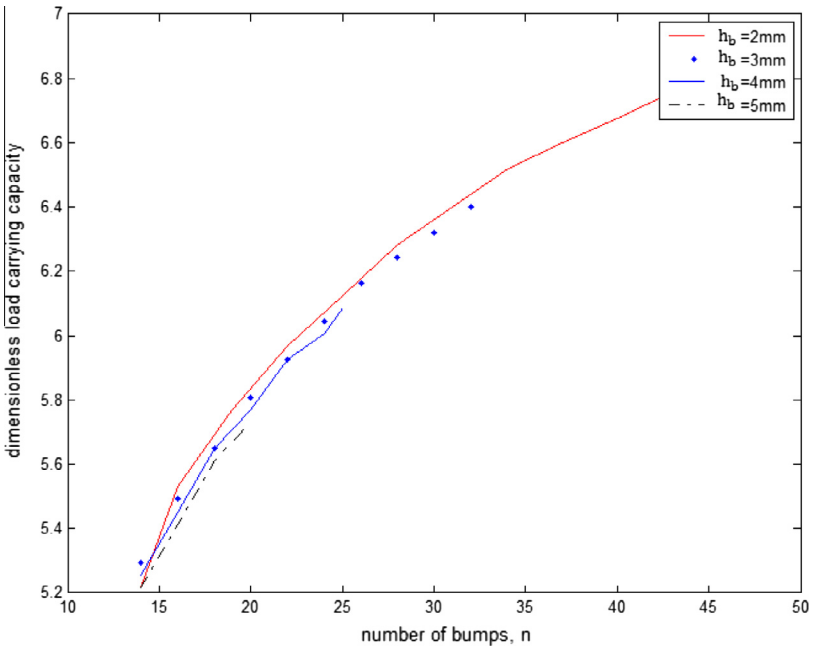

Figure 7 Effect of increasing bump height on load carrying capacity, $\varepsilon = 0.3$ and rpm = 30,000.

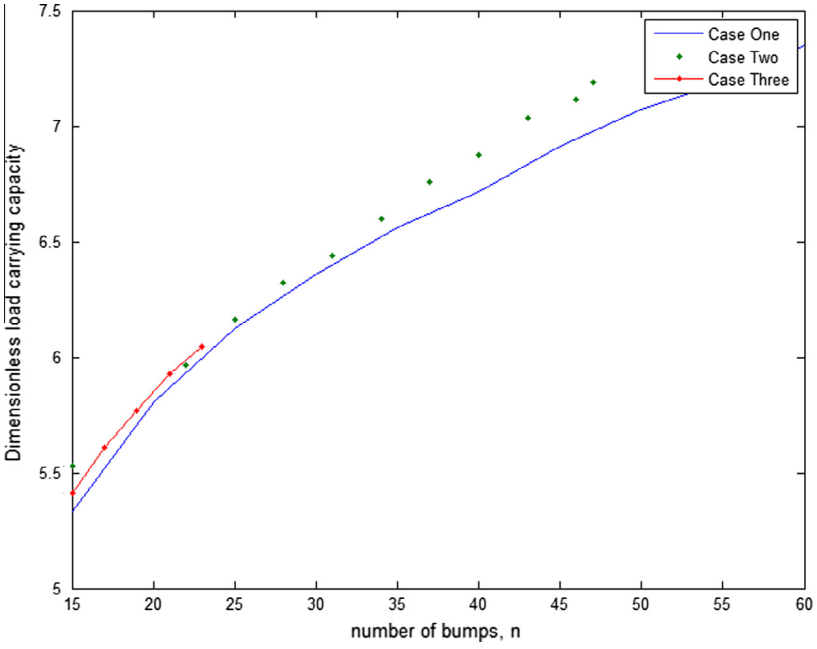

Figure 8 Effect of increasing number of bumps on bearing load carrying capacity, rpm = 30,000, $\varepsilon = 0.3$.

$$\bar{Q}_{\text{rec}} = \frac{\mu\omega L^2}{8P_a C^2}\int_0^1 \bar{h}_{cr}\partial\bar{y} - \frac{1}{12}\left(\frac{L}{D}\right)^2 \int_0^1 \bar{h}_{\text{cr}}^3 \frac{\partial\bar{P}}{\partial\theta}\bigg|_{\theta=\theta_{\text{cr}}} \partial\bar{y} \tag{14}$$

where θ_{cr} is the critical value of θ where the hydrodynamic pressure becomes subambient and $\bar{h}_{\text{cr}}$ is the dimensionless film thickness at $\theta = \theta_{\text{cr}}$.

$\bar{Q}_{\text{suc}}$ is the suction flow which is equal to the side flow and is calculated from the following integration:

$$\bar{Q}_{\text{suc}} = -\frac{1}{12}\int_0^{\theta_{\text{cr}}} \bar{h}^3 \frac{\partial\bar{P}}{\partial\bar{y}}\bigg|_{\bar{y}=0} \partial\theta \tag{15}$$

Eq. (6) is solved for pressure and repeating the calculation until convergence is achieved for a given film thickness. After some iteration using the same method of calculations and solving all the mesh points. The iterative process is carried on until the following convergence criterion is satisfied,

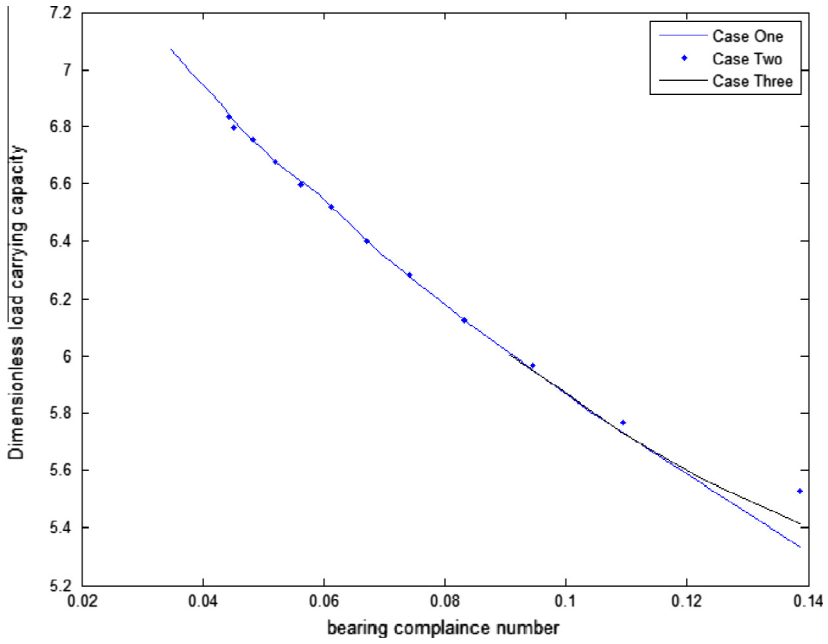

Figure 9 Effect of increasing bearing compliance number on bearing load carrying capacity, rpm = 30,000, $\varepsilon = 0.3$.

$$\frac{|(\sum \bar{P}_{i,j})_{J-1} - (\sum \bar{P}_{i,j})_J|}{|(\sum \bar{P}_{i,j})_J|} \leqslant 10^{-6}$$

After the pressure and the lubricant film profile are simultaneously determined, numerical integration is used for the load-carrying capacity calculation.

The load carrying capacity is calculated from

$$\bar{W}_x = \int_{-1}^{1} \int_{0}^{\theta_{end}} (\bar{P} - 1) \cos\theta \; d\theta d\bar{z} \tag{16}$$

$$\bar{W}_z = \int_{-1}^{1} \int_{0}^{\theta_{end}} (\bar{P} - 1) \sin\theta \; d\theta d\bar{z} \tag{17}$$

The total load-carrying capacity is given by

$$\bar{W} = \sqrt{\bar{W}_x^2 + \bar{W}_z^2} \tag{18}$$

The attitude angle (φ) is defined as

$$\tan\varphi = -\frac{\bar{W}_z}{\bar{W}_x}$$

Solving Eq. (12) and calculating $\bar{T}_{i,k}$, we combine it with Eq. (6) using mesh size of $i = 60,\ j = 20,\ k = 20$.

4. Different cases of selecting foil bearing dimensions

Tables 1 and 2 illustrate the foil bearing data used in our calculations.

The most important parameter in our study is the load carrying capacity, so we need to choose the dimensions that will guarantee high values of load carrying capacity with suitable considerations because lightly-loaded gas bearings are very unstable.

4.1. Parameters that affect the bearing performance

In order to design a foil bearing, we need to select the dimensions carefully to guarantee the highest load carrying capacity. There are many parameters that affect the bearing performance e.g. eccentricity ratio, length to diameter ratio, compliance coefficient, and bearing number.

The length of the bump is considered the most important parameter as it is the main parameter in calculating the compliance number α, which affects the pressure calculation that leads to the load carrying capacity.

First, a single bump will be considered a part of a circle as shown in Fig. 4. Generally the perimeter of the full bearing is equal to the summation of the perimeter of the whole bumps and the spaces between them, plus the thickness of the bumps:

$$n(2l + 2t_b + d) = \pi(D + 2C + 2h_b) \tag{19}$$

Also, the pitch of the bump is calculated from Eq. (20):

$$S = 2l + 2t_b + d \tag{20}$$

In our study we will assume three different cases for the foil bearing design:

- Case One: Assuming all dimensions of the bump foil are functions of half bump length l.
- Case Two: Assuming variable bump height h_b and the other dimensions of the bump height are functions of half bump length l.
- Case Three: Assuming constant housing diameter D_h and the other dimensions of the bump height are functions of half bump length l.

In Case One, we will assume the bump height, the bump thickness, and the distance between every bump and also the pitch of bump foil as follows:

- $t_b = 0.15\ l$.
- $h_b = 0.8\ l$.
- $d = 0.6\ l$.

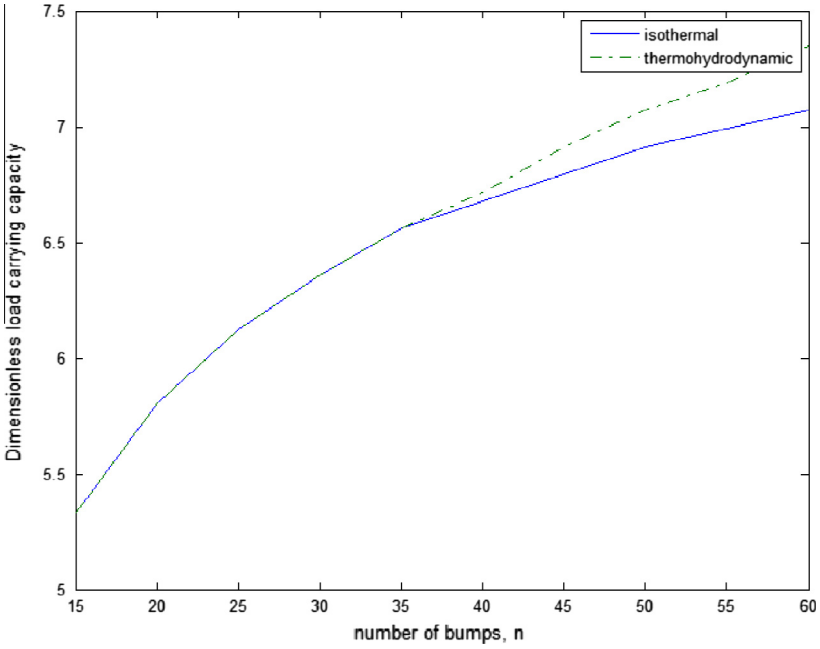

Figure 10 Case One: Effect of increasing number of bumps on bearing load carrying capacity $\varepsilon = 0.3$ and rpm = 30,000.

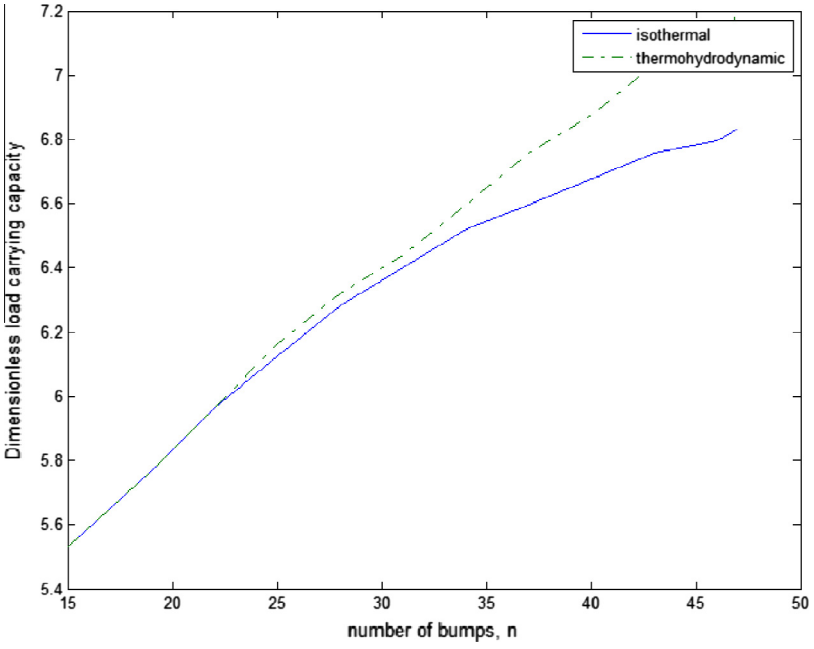

Figure 11 Case Two: Effect of increasing number of bumps on bearing load carrying capacity, $\varepsilon = 0.3$ and rpm = 30,000.

By substituting into Eq. (19)

$$l = \frac{\pi(D + 2C)}{2.9n - 1.6\pi} \tag{21}$$

A Matlab program is used to solve Eq. (21) for values of the number of bumps from 10 to 60 and the compliance number α is calculated.

Fig. 5 shows that the compliance number of the bearing decreases by increasing the number of bumps.

In Case Two, we will consider a variable bump height, and the other dimensions are functions of half bump length, so the assumptions are as follows:

- h_b = 1–8 mm.
- $d = 0.6\ l$.
- $t_b = 0.15\ l$.

By substituting in Eq. (19)

$$l = \frac{\pi(D + 2C + 2h_b)}{2.9n} \tag{22}$$

In order to determine the exact value of h_b, we will make the program stop when $h_b = r$ and that is when $2\psi = \pi$.

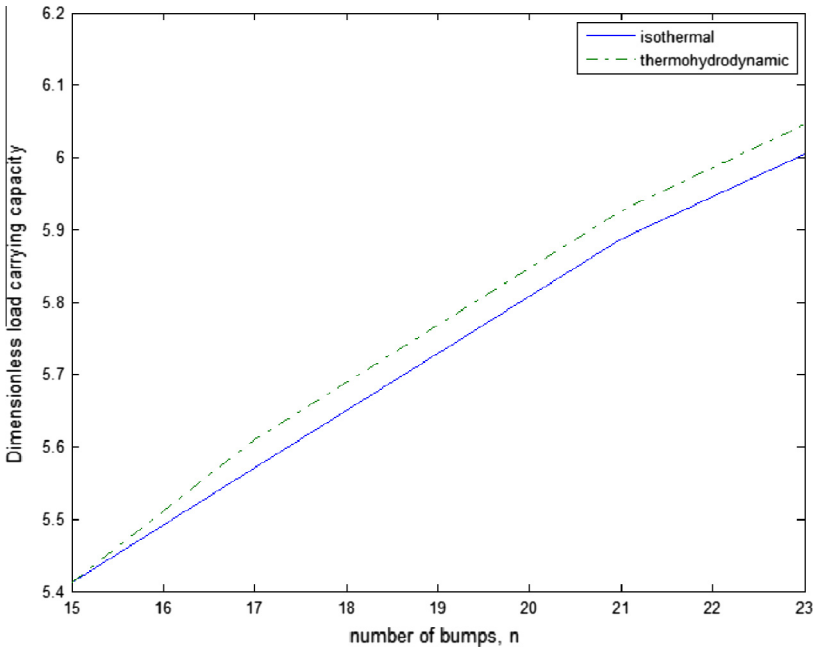

Figure 12 Case Three: Effect of increasing number of bumps on bearing load, $\varepsilon = 0.3$ and rpm = 30,000.

as

$$\cos\psi = \frac{(l+t_b)^2 - h_b^2}{(l+t_b)^2 + h_b^2} \tag{23}$$

After running the program the relation between the number of bumps, n and the compliance number, α is as shown in Fig. 6.

Fig. 6 shows that by increasing the bump height, the number of bumps decreases and the bearing compliance number also decreases.

Eq. (6) and Eq. (12) are solved using the finite difference method and the load carrying capacity (Eq. (18)) is calculated using different values of bump height. The results are as shown in Fig. 7.

Fig. 7 shows that by increasing the bump height, the dimensionless load carrying capacity decreases. It also reaches its highest value with minimum bump height.

The values where $h_b > 5$ mm are eliminated as they give imaginary numbers of pressure. Using $h_b = 1$ mm also gives imaginary numbers of pressure, so it is better to take the range of h_b from 2 mm to 5 mm.

Fig. 7 shows that it is better to take smaller values of bump height to guarantee high load carrying capacity, so $h_b = 2$ mm is the suitable value in the present design.

In Case Three, we will assume $D_h = 76$ mm and by increasing the housing diameter more than the assumed value the program will stop at less number of bumps:

$AsD_h = D + 2C + 2h_b,$

And $\pi D_h = n(2l + 2t_b + b)$ and as in Case One

- $t_b = 0.15\ l$.
- $h_b = 2$ mm.
- $d = 0.6l$.

By solving the equations of the three different cases using different values of number of bumps from 10 to 60 while keeping other parameters constants and calculating the load carrying capacity using Eq. (18), the results are as shown in Fig. 8.

For Case One, the load carrying capacity is increasing with increasing the number of bumps, but in this case there are no limitations of dimensions and the relation between parameters is selected by the reasonable design, also after running the Matlab program, we started with 15 bumps because using less than that number will lead to imaginary values of pressure.

For Case Two, the program stopped at number of bumps equal to 47 and by calculating the load within the ranged values, and it was found that it also increases with increasing the number of bumps, but if we increase the number of bumps over the ranged values, the load is still increasing, but the results are not reasonable because at this case the bump arc angle 2Ψ will be over 2π.

For Case Three, we calculated the load carrying capacity within number of bumps from 10 to 23 with constant eccentricity ratio = 0.3 and number of revolutions per minute = 30,000. In this case the load is also increasing like the two previous cases, but the values are lower than the two other values.

Fig. 9 shows that the load carrying capacity decreases with increasing the bearing compliance number, and increases with increasing the number of bumps. From Eq. (3), it is shown that the compliance number is directly proportional to the length of bump and inversely proportional to number of bumps as shown in Eq. (19).

5. Isothermal analysis

From the previous discussion, it is seen that using thermohydrodynamic analysis was found to be a little complex as we should solve Reynolds equation with the energy equation; we can simplify the analysis by using some assumptions as follows:

1. The change of pressure in the direction of air film thickness is not considered.
2. Gas flows only along circumferential direction.
3. Viscosity of flow does not change with temperature.

According to the above assumptions, the pressure distribution is expressed by Reynolds equation for compressible flow:

$$\frac{\partial}{\partial x}\left(\frac{ph^3}{\mu}\frac{\partial p}{\partial x}\right)+\frac{\partial}{\partial z}\left(\frac{ph^3}{\mu}\frac{\partial p}{\partial z}\right)=6u\frac{\partial(ph)}{\partial x} \tag{24}$$

By using dimensionless groups as follows

$$x=R\theta,\partial x=R\partial\theta,\ \bar{z}=\frac{z}{L/2},\partial z=\frac{L}{2}\bar{z},\ \bar{h}=\frac{h}{C},\ \bar{P}=\frac{p}{P_a}$$

Eq. (24) will become

$$\frac{\partial}{\partial\theta}\left(\bar{P}\bar{h}^3\frac{\partial\bar{P}}{\partial\theta}\right)+\left(\frac{D}{L}\right)^2\frac{\partial}{\partial\bar{z}}\left(\bar{P}\bar{h}^3\frac{\partial\bar{P}}{\partial\bar{z}}\right)=\Lambda\frac{\partial}{\partial\theta}(\bar{P}\bar{h}) \tag{25}$$

Using the finite difference method,
Eq. (25) becomes

$$c_1\bar{P}_{i,j}^2+c_2\bar{P}_{i,j}+c_3=0 \tag{26}$$

where

$$c_1=\bar{h}_{i,j}^3\left[\frac{2}{(\Delta\theta)^2}+\left(\frac{D}{L}\right)^2\frac{2}{(\Delta\bar{z})^2}\right]$$

$$c_2=\left[\frac{-\bar{h}_{i,j}^3\bar{P}_{i+1,j}-\bar{h}_{i,j}^3\bar{P}_{i-1,j}}{(\Delta\theta)^2}-\left(\frac{D}{L}\right)^2\frac{\bar{h}_{i,j}^3\bar{P}_{i,j+1}+\bar{h}_{i,j}^3\bar{P}_{i,j-1}}{(\Delta\bar{z})^2}+\Lambda\frac{\bar{h}_{i+1,j}-\bar{h}_{i-1,j}}{2\Delta\theta}\right]$$

$$c_3=\left[\bar{h}_{i,j}^3\frac{(\bar{P}_{i+1,j}-\bar{P}_{i-1,j})^2}{4(\Delta\theta)^2}-\left(\frac{D}{L}\right)^2\bar{h}_{i,j}^3\frac{(\bar{P}_{i,j+1}-\bar{P}_{i,j-1})^2}{4(\Delta\bar{z})^2}+\Lambda\bar{h}_{i,j}\frac{\bar{P}_{i+1,j}-\bar{P}_{i-1,j}}{2\Delta\theta}\right]$$

By solving Eq. (26) for the three different cases discussed before, the results are shown in Figs. 10–12.

For Case One, Fig. 10 shows that the load carrying capacity increases when considering the effect of temperature on Reynolds equation calculations. It also shows that the load carrying capacity increases more at higher number of bump.

For Case Two, Fig. 11 also shows that the load carrying capacity is larger for the THD case compared with the isothermal case. The load carrying capacity begins to increase more at ($n > 20$). As we noticed before this case is reasonable in calculations and for the same n, it gives higher values of load.

For Case Three, Fig. 12 shows that the load also increases in THD case, but this case gives us less range of values of number of bumps to use in calculations.

6. Conclusion

According to the previous discussion and the comparison between the isothermal and the thermohydrodynamic cases, it is clear that in order to accurately design the foil bearing, we need to study the effect of temperature of air on the bearing performance as an increase in gas temperature leads to an increase in gas viscosity; hence, it affects the foil bearing performance. On the other hand, using isothermal approach will help to simplify the solution and it also gives satisfactory results.

Also by the comparison between the three cases discussed, it is clear that assuming a variable bump height with keeping the other dimensions as functions of half bump length gives the highest values of load carrying capacity and that is the aim of the study, so Case Two is suitable for choosing the dimensions of the foil bearing. Also a wide range of number of bumps can be used, keeping the load carrying capacity as high as possible.

References

[1] H. Blok, J. Van Rossum, The foil bearing – a new departure in hydrodynamic lubrication, Lubr. Eng. 9 (6) (1953) 316–320.
[2] B.J. Patel, A. Cameron, The foil bearing, in: Proceedings of the IME, London Conference on Lubrication and Wear, Paper Number 73, 1957.
[3] W.A. Gross, Gas Film Lubrication, John Wiley and Sons, New York, 1962.
[4] A. Eshel, H.G. Elrod Jr., The theory of the infinitely wide, perfectly flexible, self-acting foil bearing, J. Basic Eng. Trans. ASME, Ser. D 87 (1965) 831–836.
[5] A. Eshel, H.G. Elrod Jr., Stiffness Effects on the Infinitely Wide Foil Bearing, ASME Paper No.66-Lub-6, January 1967, pp. 92–97.
[6] A. Eshel, Compressibility effect on the infinitely wide, perfectly flexible foil bearing, J. Lubr. Tech. 90 (1) (1968) 221–225.
[7] A. Eshel, On controlling the film thickness in self-acting foil bearings, Trans. ASME. F 92 (2) (1970) 359–362.
[8] H. Heshmat, J.A. Walowit, O. Pinkus, Analysis of gas-lubricated foil journal bearings, J. Lubr. Tech. 105 (4) (1983) 647–655.
[9] W.A. Crosby, The incompressible lubrication of a ridged foil bearing, Wear 113 (2) (1986) 247–266.
[10] C.P. Ku, H. Heshmat, Compliant foil bearing structural stiffness analysis, Part: 1. Theoretical model – including strip and variable bump foil geometry, ASME J. Tribol. 114 (2) (1992) 394–400.
[11] R. Ku, H. Heshmat, Compliant foil bearing structural stiffness analysis, ASME J. Tribol. 113 (1) (1992) 364–369.
[13] C.P. Ku, H. Heshmat, Structural stiffness and coulomb damping in compliant foil journal bearings: parametric studies, Theor. Consider. 37 (3) (1994) 525–553.
[14] C.P. Ku, H. Heshmat, Structural stiffness and coulomb damping in compliant foil journal bearings: parametric studies, Tribol. Trans. STLE Tribol. Trans. 37 (3) (1994) 455–462.
[17] Z.C. Peng, M.M. Khonsari, Hydrodynamic analysis of compliant foil bearings with compressible air flow, J. Tribol. 126 (3) (2004) 542–546.
[18] Z.C. Peng, M.M. Khonsari, A thermohydrodynamic analysis of foil journal bearings, J. Tribol. 128 (3) (2006) 534–541.
[19] E. Kuznetsov, S. Glavatskih, M. Fillon, THD analysis of a compliant journal bearings considering liner deformation, Tribol. Int. 44 (2011) 1629–1641.
[20] E.E. Swanson, Bump foil damping using a simplified model, J. Tribol. 128 (3) (2006) 542–550.
[21] C. Bhagat, L. Roy, Steady state thermo-hydrodynamic analysis of two-axial groove and multilobe hydrodynamic bearings, Tribol. Ind. 36 (4) (2014) 475–487.
[22] M. Salehi, E. Swanson, H. Heshmat, Thermal features of compliant foil bearings—theory and experiments, ASME J. Tribol. 123 (2001) 566–571.